Proceedings of the 20th International Conference on Soil Mechanics and Geotechnical Engineering– Rahman and Jaksa (Eds)

DEM modelling for geogrid-reinforced ballast

Modélisation DEM pour ballast renforcé par géogrille

Trung Ngo, Buddhima Indraratna, Yujie Qi, Chuhao Liu & Anees Siddiqui
Transport Research Center, School of Civil and Environmental Engineering, Faculty of Engineering and Information Technology, University of Technology Sydney, Australia, t*rung.ngo@uts.edu.au*

ABSTRACT: This paper presents a study to understand how the geogrid-ballast interface copes with fouling using discrete element modelling (DEM). A series of large-scale direct shear tests on fouled ballast was carried out in the laboratory under different normal stresses. DEM modelling was conducted to investigate the interface behaviour and interaction between the geogrid and ballast aggregates from micromechanical perspective. Particle shape analysis using 3D aggregate imaging and a laser scanner were introduced to construct more realistic polyhedral discrete elements that will closely represent the natural ballast particles. Geogrids were modelled by bonding small spheres together to form the desired grid geometry and apertures. Test data, including shear stress-strain responses measured from the laboratory, was used to calibrate and validate the DEM model. The DEM was then applied to insightfully investigate the contact force distributions, particle breakage, contact orientation, and the number of connectivity of ballast aggregates when subjected to shearing loads. These findings are imperative for a more insightful understanding of the load-deformation behaviour of ballast from the perspective of microstructural characteristics of discrete particle assemblies.

RÉSUMÉ : Cet article présente une étude de la façon dont l'interface géogrille-ballast fait face à l'encrassement à l'aide de la modélisation par éléments discrets (DEM). Une série d'essais de cisaillement direct à grande échelle pour les ballasts encrassés est réalisée en laboratoire sous différentes contraintes normales. La modélisation DEM est menée pour étudier le comportement de l'interface et l'interaction entre la géogrille et les agrégats de ballast d'un point de vue micromécanique. L'analyse de la forme des particules à l'aide de l'imagerie d'agrégats 3D et d'un scanner laser est introduite pour construire des éléments discrets polyédriques plus réalistes qui représenteront des particules de ballast naturelles. Les géogrilles sont modélisées en liant de petites sphères ensemble pour former la géométrie de grille et les ouvertures souhaitées. Les données de test, y compris les réponses contrainte-déformation de cisaillement mesurées à partir du laboratoire, sont utilisées pour étalonner et valider le modèle DEM. Le DEM est ensuite appliqué pour étudier de manière perspicace les distributions de force de contact, la rupture des particules, l'orientation du contact et le nombre de connectivité des agrégats de ballast lorsqu'ils sont soumis à des charges de cisaillement. Ces résultats sont impératifs pour une compréhension plus perspicace du comportement charge-déformation du ballast du point de vue des caractéristiques microstructurales des assemblages de particules discrètes.

KEYWORDS: ballast, coal fines, discrete element method, geogrid, rail geotechnics.

1 INTRODUCTION

Given that the current Australian ballasted tracks in many places cannot cater to heavy hauls and freight trains, the need to develop an innovative and sustainable railroad for transport infrastructure is crucial. This has intensified pressure on the railway industry to find creative solutions and use cutting edge technology to maintain track stability and reduce maintenance costs (Selig and Waters 1994, Sayeed and Shahin 2017, Indraratna et al. 2020). A typical track substructure consists of a ballast layer, a compacted layer of capping (sub-ballast) placed above a formation soil and a coarse granular medium (ballast) placed over the sub-ballast. The main functions of capping layers are transmitting and distributing the dynamic train wheel loads from the sleepers and ballast to the formation soils at reduced and acceptable stress stages. Capping materials commonly consist of broadly-graded mixtures of sand and gravel meant to prevent coarse ballast aggregates from penetrating into the sub-base and reduce the possibility of fines from the underlying subgrade soils migrating upwards into the ballast. Besides, the capping also acts like a filter and a separating layer, thus preventing excess pore pressure built up and facilitating track drainage. Subject to cyclic loading by trains, the granular aggregates gradually degrade and lose their shear strength and drainage capacity. The ballast, which is a significant component of the conventional railway tracks, can absorb a large proportion of the dynamic load and thereby offers desirable resiliency to repeated wheel loads. However, ballast aggregates degrade and settle upon repeated loading from the moving train, and as a result, differential settlements will occur along the track. To maintain track stability and improve passenger comfort, the settlements must be kept within certain limits, and this can be done by reinforcing the ballast bed with geogrids (Shin et al. 2002, Brown et al. 2007, Fernandes et al. 2008, Indraratna et al. 2016, Dong et al. 2010, Ngo et al. 2017).

Loss of track geometry due to excessive differential settlements and localised failures of formation (capping and subgrade) often result in the loss of stability and longevity of rail tracks. In this regard, planer geosynthetics (geogrids, geo-composites, geocells, rubber mats) have been widely adopted to mitigate excessive track settlements and lateral displacements under cyclic train loading (Bathurst and Raymond 1987, McDowell and Stickley 2006, Tutumluer et al. 2012, Biabani et al. 2016, Jayasuriya et al. 2019). Geogrids have been widely used to stabilise the substructure of rail tracks (Bathurst and Raymond 1987; Ashmawy and Bourdeau 1995; Fernandes et al. 2008, Ngo et al. 2014). It was known that geosynthetics provided additional confinement onto the granular layers and thus restrained deformation of track substructure. A geogrid is a type of planar geosynthetics which is commonly used to provide lateral and vertical constraints to ballast aggregates. Due to the interlocking with surrounding grains, the geogrid acts presumably as a non-displacement boundary that confines particles via the interlocking and frictional resistance. As a result, the inclusion of geogrid could decrease particle displacements.

2 LABORATORY TESTS

2.1 *Large-scale direct shear tests of geogrid-reinforced ballast*

The large-scale direct shear box used for the experiments consists of a 300 × 300 mm^2 square steel box, and 200 mm-high. Ballast particles with appropriate sizes and distributions were compacted into layers of 50 mm-thick to the field unit weight of 15.5 kN/m^3. A layer of geogrid (aperture size: 40mm × 40mm) was placed in the middle between the lower and upper compartment of the shear box and secured firmly to the apparatus. The apparatus applied the normal stress via a rigid and free plate placed on the top of the shear box using a deadweight system attached to a lever arm. Direct shear tests were conducted at four normal stresses of σ_n=15, 27, 51 and 75 kPa. The apparatus forced the lower half of the shear box to shear horizontally by an electric motor at a velocity of 1.25 mm/minute up to a maximum displacement of 37 mm (approximate shear strain, ε_s=13%) while the upper half of the box remained stationary. During the tests, the device recorded shearing forces and vertical displacements of the top plate (vertical strain) at a given shear strain. Based on extensive tests, the results show that the peak shear stress increased non-linearly, with an increase in normal stress, but then it decreased as the ballast aggregates became degraded and fouled. While detailed experimental results were reported earlier by Indraratna et al. (2011), some of these test results are adopted in this study to calibrate and validate the DEM model.

3 DISCRETE ELEMENT MODELLING

Past literature has investigated the performance of geogrid-reinforced ballast (e.g., Fernandes et al. 2008; Indraratna et al. 2019; Pokharel et al. 2010; Ngo and Indraratna et al. 2016, Sugimoto & Alagiyawanna 2003). However, researchers conducted most of the studies in the laboratory. They only made limited attempts to study the reinforcement effects of geogrid numerically, especially the interlocking mechanism of discrete aggregate and the geogrid. The discrete element method (DEM) based on discrete particle mechanics firstly developed by Cundall and Strack (1979) has been adopted rapidly as it can simulate more insightful micro-mechanical responses of granular aggregates (i.e., Cheng et al. 2004, Nakata et al. 2005, McDowell et al. 2006, Tutumluer et al. 2006, O'Sullivan 2011, Ngo et al. 2017). Also, the DEM approach can supply micro-mechanical information, consisting of contact force chains, particle velocities/displacements, particle breakage and evolutions of fabric that are very difficult to measure experimentally (Rothenburg and Bathurst 1992, Pan and Dong 1999, O'Sullivan et al. 2008). The current study is an attempt to use DEM to predict the shear stress-strain responses and micro-mechanical analysis of ballast with and without the inclusion of geogrid.

3.1 *DEM for geogrid-reinforced ballast*

Modelling a geogrid in DEM is a challenging task due to the complex geometry and flexibility of the geogrid. In this study, a biaxial geogrid was modelled by bonding several spherical balls (radius: r_b=2.0mm - 4.0mm) together by parallel bonds (Fig. 1). These balls were connected by parallel bond strengths, corresponding to geogrid's tensile strength in elastic range and was determined by conducting tensile tests in the laboratory. These bonds form an elastic interaction between ballast that can transmit both forces and moments.

The total force and moment associated with the parallel bond are denoted by $\overline{F_i}$ and $\overline{M_i}$, with the convention that this force and moment represent the action of the adhesive on particles. It can resolve each of these vectors into normal and shear components for the contact.

$$\overline{F_i} = \overline{F_i}^n + \overline{F_i}^s \quad (1)$$

$$\overline{M_i} = \overline{M_i}^n + \overline{M_i}^s \quad (2)$$

The force-increments occurring over a timestep (Δt) are computed by:

$$\text{Normal force: } \Delta\overline{F_i}^n = \left(-\overline{k}_n A \Delta U_i^n\right) n_i \quad (3)$$

$$\text{Shear force: } \Delta\overline{F_i}^s = -\overline{k}_s A \Delta U_i^s \quad (4)$$

The increments of the moment are determined by:

$$\Delta\overline{M_i}^n = \left(-\overline{k}_s J \Delta\theta_i^n\right) n_i \quad (5)$$

$$\Delta\overline{M_i}^s = -\overline{k}_n I \Delta\theta_i^s \quad (6)$$

with, $\Delta\theta_i = \left(\omega_i^{[B]} - \omega_i^{[A]}\right)\Delta t$

where, ΔU_i^n and ΔU_i^s: normal and shear relative displacement increments; $\Delta\theta_i^n$ and $\Delta\theta_i^s$: normal and shear relative rotation increments, respectively; A, J and I are the area, polar moment and moment of inertia of the bond cross-section, respectively, and are defined as functions of the radius $\overline{R}$ of the bonding disk between spheres, as given:

$$A = \pi\overline{R}^2; \quad I = \frac{1}{2}\pi\overline{R}^4; \quad \text{and} \quad J = \frac{1}{4}\pi\overline{R}^4 \quad (7)$$

The maximum normal stress (σ_{max}) and shear stress (τ_{max}) acting on the bond are calculated by:

$$\sigma_{max} = \frac{-\overline{F_i}^n}{A} + \frac{\left|\overline{M_i}^s\right|}{I}\overline{R} \quad (8)$$

$$\tau_{max} = \frac{\left|\overline{F_i}^s\right|}{A} + \frac{\left|\overline{M_i}^n\right|}{J}\overline{R} \quad (9)$$

If either of these maximum stresses exceeds its corresponding bond strength, the parallel bond breaks, and this is considered to be related to the breaking of geogrid.

To model ballast aggregates in DEM, particle shape analysis using 3D aggregate imaging and a laser scanner were used to construct a library of realistic polyhedral discrete elements that could represent natural ballast particles. Irregularly-shaped ballast grains were then simulated by the clumping of many balls together in predetermined positions and sizes to fill up the polyhedral meshes, as shown in Figure 2a. Mathematical equations for the motion of a clump were described by Itasca (2016) where a clump was treated as a rigid body and interacts with others at pair-wise contacts. The movement of a clump was then determined by the resultant force (**F**) and moments (**M**) acting upon it, as given below:

$$\mathbf{F} = \tilde{F} + \sum_{p=1}^{N_p}\left(\widetilde{F_{[p]}} + \sum_{c=1}^{N_c} F_{[p,c]}\right) \quad (10)$$

where, $\tilde{F}$ is the externally applied force acting on the clump; $\widetilde{F_{[p]}}$ is the externally applied force acting on the particle *(p)*; and $F_{[p,c]}$ is the force acting on the particle *(p)* at contact *(c)*.

The resultant moment, **M** is determined by:

$$\boldsymbol{M} = \widetilde{M} + \sum_{p=1}^{N_p}\left(\widetilde{M_{[p]}} + \epsilon_{ijk}\left(x_{[p]}^j - x_c^j\right)F_{[p]}^k + \sum_{c=1}^{N_c}\epsilon_{ijk}\left(x_{[c]}^j - x_{[p]}^j\right)F_{[p,c]}^k\right) \quad (11)$$

where, $\widetilde{M}$ is the externally applied moment acting on the clump; $\widetilde{M_{[p]}}$ is the externally applied moment acting on a particle *(p)*; $F_{[p]}^k$ is the resultant force acting on the particle *(p)* at its centroid; $F_{[p,c]}^k$ is the force acting on a particle *(p)* at contact *(c)*; and ϵ_{ijk} is the permutation symbol, given by:

$$\epsilon_{ijk} = \begin{cases} 0, & \text{if 2 indices coincide;} \\ +1, & \text{if } i,j,k \text{ permute like } 1,2,3; \\ -1, & \text{otherwise.} \end{cases} \quad (12)$$

Figure 2b presents a DEM model of large-scale direct shear test for ballast sample with the inclusion of the geogrid in the middle of the shear box. In DEM, the density and compaction level were maintained as same as experimental tests by controlling the porosity of a simulated granular assembly. Particles were generated in the shear box at random orientations to resemble experimental conditions. The void ratio of the assembly representing the initial condition of the test specimen was controlled at 0.82 (i.e. porosity of 45%). Figure 2c shows an image of a small sample of the geogrid tested in the laboratory. Parameters used to simulate granular aggregates in DEM were selected by calibrating the DEM-based shear stress-strain responses of the material with the laboratory measurements. A set of parameters initially adopted from existing research was used to simulate the ballast in DEM (Lobo-Guerrero and Vallejo 2006, Huang et al. 2008, Lu and McDowell 2010, Tutumluer et al. 2012, Suhr et al. 2018, Guo et al. 2020). Authors then modified these parameters gradually until the predicted shear stress-strain responses matched reasonably well with those already reported. Once a given set of micro-mechanical parameters was adequately calibrated (Table 1), we then used them to simulate the large-scale direct shear tests for ballast (with and without the geogrid).

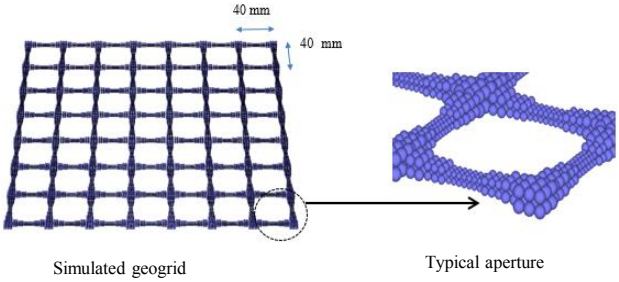

Figure 1. DEM modelling of a typical geogrid used in the laboratory test (modified after Ngo et al. 2017)

Table 1. Micromechanical parameters used in DEM analysis

Parameter	Geogrid	Ballast
Particle density (kg/m^3)	972	2550
Coefficient of friction	0.47	0.85
Contact normal stiffness (N/m)	5.91×10^6	4.82 E8
Contact shear stiffness (N/m)	5.91×10^6	2.41 E8
Contact normal stiffness of wall-particle (N/m)	3.25×10^9	3.25 E9
Shear stiffness of wall of wall-particle (N/m)	3.25×10^9	3.25 E9
Parameter of contact bond shear strength, ϕ_s (kN)	6.27×10^7	
Parallel bond radius multiplier	0.5	
Parallel bond normal stiffness (kPa/m)	452×10^7	
Damping ratio	0.7	0.7

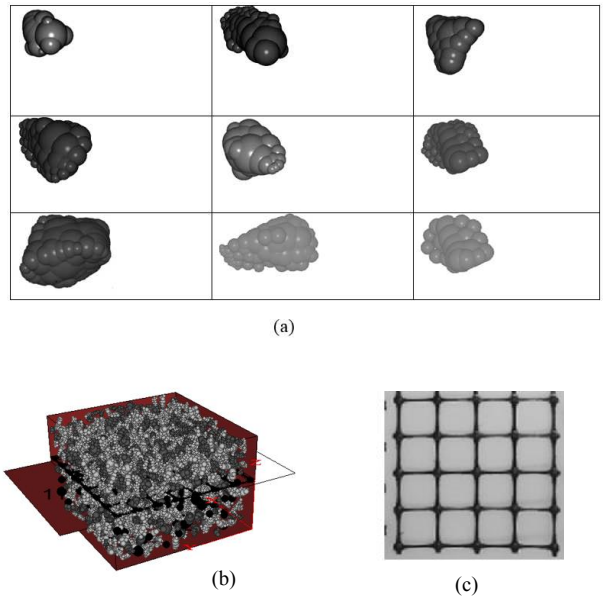

Figure 2. (a) Library of ballast particle shapes modelled in DEM; (b) DEM model for direct shear box; (c) Geogrid tested in the laboratory (*modified after Ngo et al. 2017*)

4 RESULTS AND DISCUSSION

4.1 *Shear stress-strain responses*

The authors have carried out the experimental program and DEM simulations for fresh ballast reinforced by geogrid out at three normal stresses of σ_n = 27kPa, 51kPa, and 75kPa. Figure 3 presents comparisons between the DEM simulation and experimental results of shear stress-strain for a ballast assembly with and without the inclusion of geogrid. Overall, the DEM results reasonably agree with the measured experimental data for any given normal stress σ_n. Simulation captured strain-softening responses whereby the higher normal stress, the more significant peak shear stress as expected. This strain-softening behaviour of the ballast grains follows a similar trend with other rock-fill aggregates of similar sizes (Marsal 1973, Charles & Watts 1980). Compared to experimental data, the DEM simulations exhibit a particular discrepancy in the stress-strain responses at a shear strain of 3-7%. This difference may be associated with any grain breakage that could not be precisely simulated in the DEM, and the rigidity of the loading plate. Besides, the discrepancy in the shear stress-strain response can also be due to the reduction of interlocking provided by the irregular shape of ballast aggregates, which influences the rolling resistance and re-arrangement of aggregates.

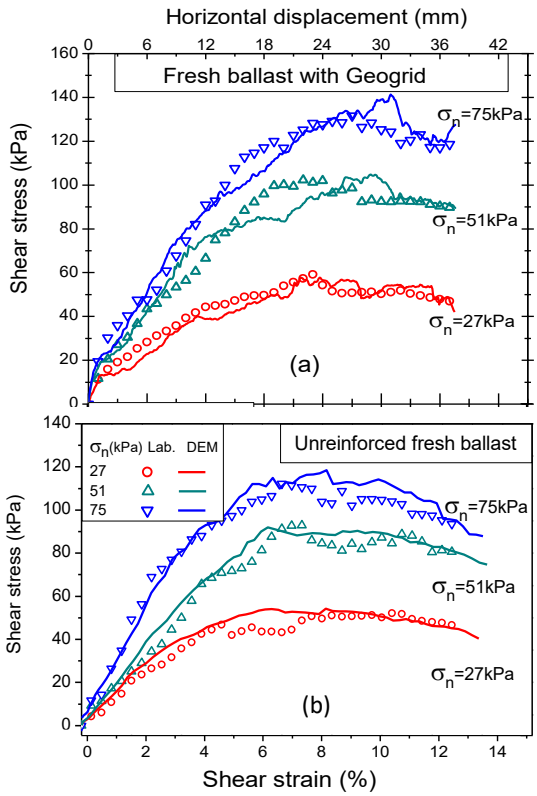

Figure 3. Comparisons of shear stress-strain and the volumetric response of fresh ballast between experiment and DEM simulation (*modified after Ngo et al . 2014*)

4.2 *Contact force distribution and orientation*

Figure 4 presents the contact force distributions inside ballast assembly with and without the inclusion of a geogrid predicted at a shear strain of ε_s = 5% and under given normal stress of σ_n = 51 kPa. The authors plotted contact forces between particles as solid lines where the thickness of each line is proportional to the magnitude of the contact forces. For brevity, only forces with a magnitude more massive than average forces in the assembly were presented. The geogrid-stabilised ballast showed a denser contact force distribution (i.e., a higher number of contacts) and lesser maximum contact force compared to those for the unreinforced ballast assembly. Indeed, with the inclusion of geogrid, there are a total of N_c=36,741 contacts, and authors observed the maximum contact force of F_{max}= 126 N in comparison of N_c=32,385 contacts and F_{max}= 157 N for the case of unreinforced. It is also seen that at the shearing plane, contact forces developed between the geogrid and surrounding ballast grains associated with a significantly increased number of contact forces, which are attributed to the interlocking effect occurring between them. The increased N_c would help partially carry and transmit contact forces across the assembly, and as a result, it can form more uniform contact force. Also, simulation measured the high maximum contact forces for an unreinforced case, and this may lead to the crushing of single ballast particles under shearing stresses.

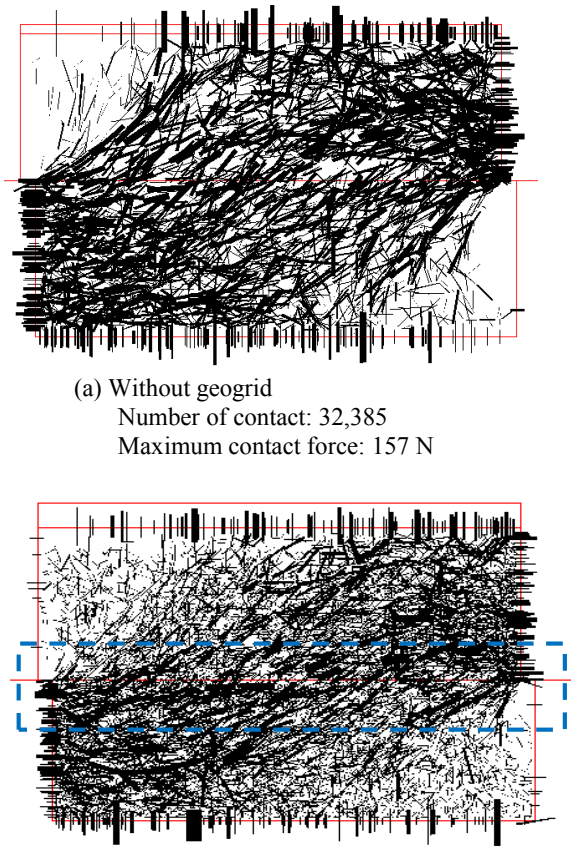

(a) Without geogrid
Number of contact: 32,385
Maximum contact force: 157 N

(b) With geogrid
Number of contact: 36,741
Maximum contact force: 126 N

Figure 4. Distribution of contact force captured at a shear strain of ε_s=5%: (a) unreinforced ballast; (b) geogrid-unreinforced ballast (*modified after Ngo et al . 2014*)

Figure 5 shows the distributions of the mean contact forces along the depth of a shear box for unreinforced and geogrid-reinforced ballast specimens at a shear strain of $\varepsilon_s = 5\%$ and a normal stress of $\sigma_n = 51$ kPa. It is evident that the unreinforced ballast exhibits smaller mean contact forces compared to those for the geogrid-reinforced ballast. Indeed, at the middle of the shearing box and with the present of geogrid, the simulation predicted the mean contact force as about 49.2 N compared to 24.5 N for the case of unreinforced, which reached of approximately three times compared to those that are close to the top and bottom of the shear box. A confinement zone of geogrid was formed within a depth of around h_{conf} = 50 mm on both sides of the geogrid-ballast interfaces where the inclusion of geogrid leads to a considerable increase in developed contact forces. The strong mechanical interlock between the geogrid and ballast grains provided this mobilisation of large contact forces within the confinement zone of geogrids.

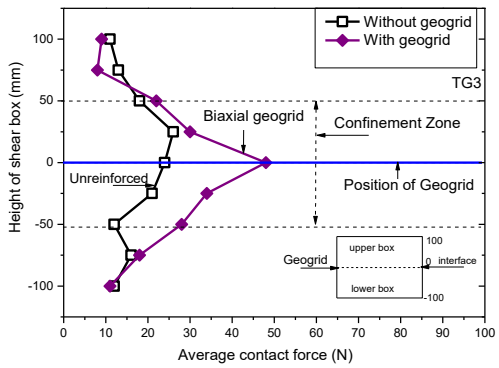

Figure 5. Average contact force of ballast specimens subjected to a shear strain of ε_s=5%

The force-fabric is characterised by the distribution of inter-particle contact orientations, which can be represented by the Fourier series approximations proposed by Rothenburg and Bathurst (1989),

$$E(\theta) = \frac{1}{2\pi}[1 + a\cos 2(\theta - \theta_r)] \quad (13)$$

where, a *is* the coefficients of contact and θ_r is the corresponding major principal directions of contact anisotropy. Figure 6 illustrates polar histograms of contact orientation for unreinforced and geogrid-reinforced ballast captured in DEM simulation at a given shear strain of ε_s = 10%. Counting contact force information at the predefined bin angle, $\Delta\theta$=10°, determined the polar histograms of the contact forces. The contact force orientations of both unreinforced and reinforced ballast exhibit a predominant distribution in the vertical direction. Subjected to shearing, contact force chains develop to resist shear and disperse the loads from the surface into ballast grains. Anisotropies of contact forces rotate significantly during shearing progress. It is predicted that while the contact orientation in the unreinforced ballast assembly exhibits a principal direction of around θ_r = 29°, the geogrid-reinforced ballast assemblies showed contact orientations of about θ_r = 16°. It means that there were more contacts formed in the vertical direction, and this could be related to the interlocking effect of the geogrid. On the other hand, the inclusion of geogrids results in an increased number of contacts in the vertical directions that may cause a change in the fabric anisotropy of contact. It is believed that the inherent anisotropy affects the overall shear strength of ballast assemblies. Therefore, understanding the contact force distribution in the ballast assemblies and its evolution is most beneficial, and it provides more insight into the orientation of contacts transmitted in ballast assemblies.

4.3 *Contour of strains developed in the geogrid*

Strain gauges are often used to measure strain mobilised in geogrid during laboratory tests. However, due to some difficulties in installing and protecting strain gauges from the damage caused by sharp edges of aggregates, strains in the geogrid could not be measured accurately in the laboratory tests. Taking advantage of numerical modelling through DEM simulations, it can capture strains developed across the geogrid in the horizontal shearing direction in this study. Figure 7 shows the contour of strain in the geogrid at the end of the shear test captured in a horizontal direction. It is observed that the strains developed non-uniformly across the geogrid, and the magnitude of strain may depend on the degree of interlock occurring between the geogrid and ballast aggregates (Ngo et al. 2014). The maximum strain mobilised in the geogrid was measured around 1.2%.

5 CONCLUSIONS

This study has carried out a set of large-scale direct shear tests on track ballast with and without the inclusion of a biaxial geogrid. Authors used some of the laboratory test data to calibrate and validate the numerical modelling phase. Authors also conducted numerical modelling through the use of discrete element method (DEM) considering the reinforcement effects of geogrids. Ballast aggregates were simulated by bonding many spheres together to form appropriate sizes and shapes. A biaxial geogrid was modelled in the DEM by connecting small balls to make regular opening aperture as the tested geogrid.

Following the laboratory test procedure, we have implemented DEM simulations for large-scale shear tests of ballast with and without geogrid. The results of shear stress-strain responses predicted from DEM simulations were in good agreement with those measured experimentally, which indicated that the DEM model could be adopted to predict the stress-strain responses of ballast. This study used the DEM model to predict the micro-mechanical responses of geogrid-reinforced ballast assemblies, including contact force distributions, contact orientation and contour strains developed across the geogrid. Simulation results showed that the inclusion of geogrid increased the number of contact forces and decreased the maximum contact forces which can be used to justify the benefit of geogrid given reducing the displacement and breakage of ballast aggregates. Distributions of average contact forces with the depth of shear box with and without the inclusion of geogrid were captured showing that the geogrid-reinforced ballast had the highest mobilised contact forces at the middle of the shear box (interface). Contour strains mobilised across the geogrids in a horizontal shearing direction were also captured, and the highest strain mobilised in the geogrid was predicted at about 1.2%.

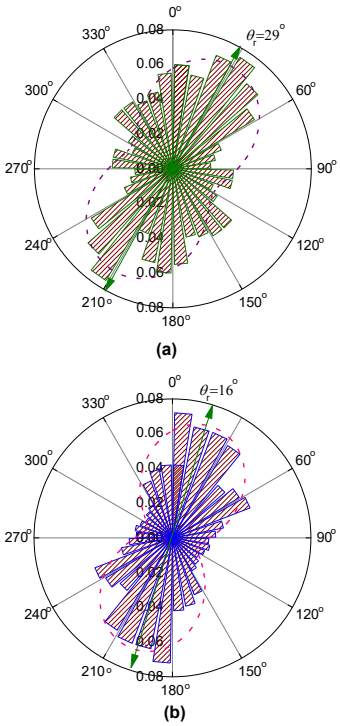

Figure 6. Contact force orientations of ballast at the shear strain of ε_s=10%: (a) without geogrid; (b) with geogrid

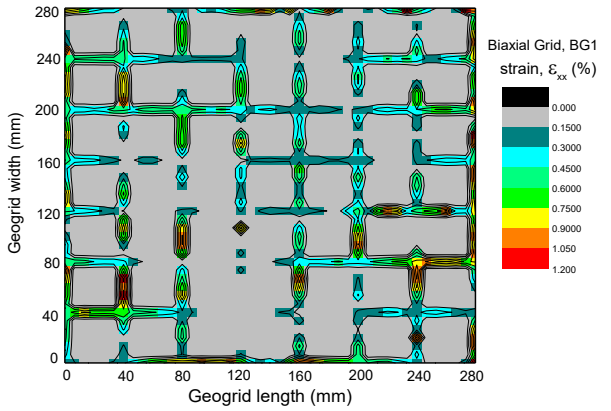

Figure 7. Predicted contour strains developed across the geogrid at a shear strain of ε_s=10%

6 ACKNOWLEDGEMENTS

The authors much appreciate the financial support provided by the Australian Government through the ITTC-Rail (IC170100006). Some research outcomes were reproduced in this paper with kind permission from the ASCE-International Journal of Geomechanics, Granular Matters and Computer and Geotechnics.

7 REFERENCES

Ashmawy A.K. and Bourdeau P. L. 1995. Geosynthetic-reinforced soils under repeated loading: A review and comparative design study. *Geosynthetics International* 2(4), 643-678.

Bathurst R.J. and Raymond G.P. 1987. Geogrid reinforcement of ballasted track. *Transportation Research Record* 1153, 8-14.

Biabani M.M. Ngo N.T. and Indraratna B. 2016. Performance evaluation of railway subballast stabilised with geocell based on pull-out testing. *Geotextiles and Geomembranes* 44(4), 579-591.

Brown S.F. Kwan J. and Thom N.H. 2007. Identifying the key parameters that influence geogrid reinforcement of railway ballast. *Geotextiles and Geomembranes* 25(6), 326-335.

Charles and Watts (1980). The influence of confining pressure on the shear strength of compacted rockfill. *Géotechnique* 30(4), 353-367.

Cheng, Bolton and Nakata Y. 2004. Crushing and plastic deformation of soils simulated using DEM. *Géotechnique* 54(2), 131-141.

Cundall P.A. and Strack O.D.L. 1979. A discrete numerical model for granular assemblies. *Géotechnique* 29 (1), 47-65.

Dong Y.L. Han J. and Bai X.H. 2010. A numerical study on stress-strain responses of biaxial geogrids under tension at different directions. *GeoFlorida 2010: Advances in Analysis, Modeling & Design, ASCE* (GSP 199), 2551-2560.

Fernandes G. Palmeira E.M. and Gomes R.C. 2008. Performance of geosynthetic-reinforced alternative sub-ballast material in a railway track. *Geosynthetics International* 15(5), 311-321.

Guo Y. Zhao C. Markine V. Jing G. and Zhai W. 2020. Calibration for discrete element modelling of railway ballast: A review. *Transportation Geotechnics* 23: 100341.

Huang Z.Y. Yang Z.X. and Wang Z.Y. 2008. Discrete element modeling of sand behavior in a biaxial shear test. *Journal of Zhejiang University SCIENCE A* 9(9), 1176-1183.

Indraratna B. Ngo N.T. and Rujikiatkamjorn C. 2011. Behavior of geogrid-reinforced ballast under various levels of fouling. *Geotextiles and Geomembranes* 29(3), 313-322.

Indraratna B. Ngo T. Ferreira, Rujikiatkamjorn C. and Shahkolahi A. 2020. Laboratory examination of ballast deformation and degradation under impact loads with synthetic inclusions. *Transportation Geotechnics* 25: 100406.

Indraratna, B., Qi, Y., Ngo, T.N., Rujikiatkamjorn, C., Neville, T., Ferreira, F. B. and Shahkolahi, A. 2019. Use of geogrids and recycled rubber in railroad infrastructure for enhanced performance. *Geosciences* 9(1), 30.

Indraratna, B., Nimbalkar, Ngo N.Y. and Neville T. 2016. Performance improvement of rail track substructure using artificial inclusions: Experimental and numerical studies. *Transportation Geotechnics* 8, 69-85.

Itasca 2016. Particle flow code in three dimensions (PFC3D). Itasca Consulting Group, Inc., Minnesota.

Jayasuriya, C., Indraratna and Ngo T. 2019. Experimental study to examine the role of under sleeper pads for improved performance of ballast under cyclic loading. *Transportation Geotechnics* 19, 61-73.

Lobo-Guerrero, S. and Vallejo L.E. 2006. Discrete element method analysis of railtrack ballast degradation during cyclic loading. *Granular Matter* 8(3-4), 195-204.

Lu, M. and McDowell G.R. 2010. Discrete element modelling of railway ballast under monotonic and cyclic triaxial loading. *Géotechnique* 60(6), 459-467.

Marsal R.J. 1973. Mechanical properties of Rockfill. In : Embankment Dam Engineering Wiley, New York, pp: 109-200.

McDowell G.R., Harireche O. Konietzky H. Brown S.F. and Thom N.H. 2006. Discrete element modelling of geogrid-reinforced aggregates. *Proceedings of the ICE - Geotechnical Engineering* 159(1), 35-48.

McDowell G.R. and Stickley P. 2006. Performance of geogrid-reinforced ballast. *Ground Engineering* 1(1), 26-33.

Nakata, Y. Bolton M.D. Cheng Y.P. 2005. Relating particle characteristics to macro behavior of DEM crushable material. Powders and grains,: Garcia-Rojo, Herrmann and McNamara (eds), Taylor & Francis Group, London, 1387-1391.

Ngo T, Indraratna B., and Rujikiatkamjorn C., 2014. DEM simulation of the behaviour of geogrid stabilised ballast fouled with coal. *Computers and Geotechnics*, 55: 224-231.

Ngo T. Indraratna B. and Rujikiatkamjorn C. 2017. Stabilisation of track substructure with geo-inclusions: experimental evidence and DEM simulation. *International Journal of Rail Transportation* 5(2), 63-86.

Ngo N.T. Indraratna B. and Rujikiatkamjorn C. 2017. A study of the geogrid-subballast interface via experimental evaluation and discrete element modelling. *Granular Matter* 19(3), 1-16.

O'Sullivan, C. 2011. Particulate Discrete Element Modelling: A Geomechanics Perspective, Spon press, London.

O'Sullivan C. Cui L. and O'Neill C. 2008. Discrete element analysis of the response of granular materials during cyclic loading. *Soils and Foundations* 48(4), 511-530.

Pan Y.W. and Dong J.J. 1999. A micromechanics-based methodology for evaluating the fabric of granular material. *Géotechnique* 49(6), 761-775.

Rothenburg L. and Bathurst R.J. 1989. Analytical study of induced anisotropy in idealised granular materials. *Géotechnique* 39(4), 601-614.

Rothenburg, L. and Bathurst R.J. 1992. Micromechanical features of granular assemblies with planar elliptical particles. *Géotechnique* 42(1), 79-95.

Sayeed M.A. and Shahin M.A. 2017. Design of ballasted railway track foundations using numerical modelling. Part I: Development. *Canadian Geotechnical Journal* 55(3), 353-368.

Selig E.T. and Waters J.M. 1994. Track geotechnology and substructure management, Thomas Telford, London.

Shin, E.C. Kim D.H. and Das B.M. 2002. Geogrid-reinforced railroad bed settlement due to cyclic load. *Geotechnical and Geological Engineering* 20, 261-271.

Suhr B. Marschnig S. and Six K. 2018. Comparison of two different types of railway ballast in compression and direct shear tests: experimental results and DEM model validation. *Granular matter* 20(4), 70-70.

Sugimoto M. and Alagiyawanna A.N. 2003. Pullout behavior of geogrid by test and numerical analysis. *Journal of Geotechnical and Geoenvironmental Engineering* 129(4), 361-371.

Tutumluer E. Huang H. and Bian X. 2012. Geogrid-aggregate interlock mechanism investigated through aggregate imaging-based discrete element modeling approach. *International Journal of Geomechanics* 12(4), 391-398.

Tutumluer E. Huang H. Hashash Y. and Ghaboussi J. 2006. Aggregate shape effects on ballast tamping and railroad track lateral stability. Proceedings of the 2006 AREMA Annual Conference, Louisville, Kentucky